ACS APPLIED MATERIALS & INTERFACES

Research Article

www.acsami.org

Electrospun Superhydrophobic Organic/Inorganic Composite Nanofibrous Membranes for Membrane Distillation

Xiong Li, Xufeng Yu, Cheng Cheng, Li Deng, Min Wang, and Xuefen Wang*

State Key Lab for Modification of Chemical Fibers and Polymer Materials, Donghua University, Shanghai 201620, People's Republic of China

Supporting Information

ABSTRACT: Electrospun superhydrophobic organic/inorganic composite nanofibrous membranes exhibiting excellent direct contact membrane distillation (DCMD) performance were fabricated by a facile route combining the hydrophobization of silica nanoparticles (SiO_2 NPs) and colloid electrospinning of the hydrophobic silica/poly(vinylidene fluoride) (PVDF) matrix. Benefiting from the utilization of SiO_2 NPs with three different particle sizes, the electrospun nanofibrous membranes (ENMs) were endowed with three different delicate nanofiber morphologies and fiber diameter distribution, high porosity, and superhydrophobic property, which resulted in excellent waterproofing and breathability. Significantly, structural attributes analyses have indicated the major contributing role of fiber diameter distribution on determining the augment of permeate vapor flux through regulating mean flow pore size (MFP). Meanwhile, the extremely high liquid entry pressure of water (LEPw, 2.40 ± 0.10 bar), robust nanofiber morphology of PVDF immobilized SiO_2 NPs, remarkable mechanical properties, thermal stability, and corrosion resistance endowed the as-prepared membranes with prominent desalination capability and stability for long-term MD process. The resultant choreographed PVDF/silica ENMs with optimized MFP presented an outstanding permeate vapor flux of 41.1 kg/(m^2·h) and stable low permeate conductivity (~2.45 μs/cm) (3.5 wt % NaCl salt feed; ΔT = 40 °C) over a DCMD test period of 24 h without membrane pores wetting detected. This result was better than those of typical commercial PVDF membranes and PVDF and modified PVDF ENMs reported so far, suggesting them as promising alternatives for MD applications.

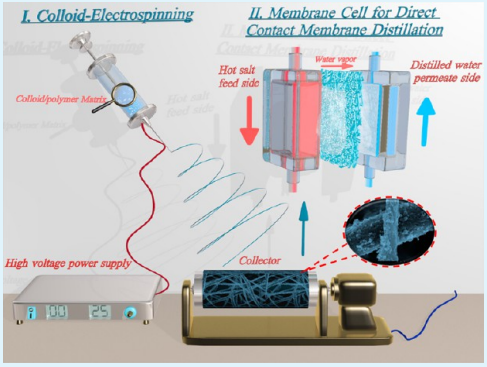

KEYWORDS: *colloid electrospinning, silica nanoparticles, superhydrophobicity, nanofibrous membrane, membrane distillation*

INTRODUCTION

With water scarcity occurring globally in our time, inadequate access to safe drinking water has become one of the most pervasive problems afflicting people throughout the world,[1] and the surging population growth, industrialization, contamination of available freshwater resources, and climate change will further aggravate the challenge of providing ample potable water.[2] Seawater and brackish water reverse osmosis (RO), the dominant membrane-based technology for desalination, has been developed considerably for the production of high quality water over the past 4 decades due to improved membrane materials and decreased costs.[3,4] However, the energy consumption of RO technology still has to be substantially reduced, and the existence of potentially adverse environmental impacts, such as the emission of air pollutants and greenhouse gases, further exacerbate climate change.[2] Notably, these limitations of the RO process can be avoided by another membrane-based process, membrane distillation (MD) technology, which is a thermally driven nonisothermal membrane separation process, in which only vapor molecules can transfer through a highly hydrophobic microporous membrane. The driving force in the MD process is the vapor pressure difference induced by the temperature difference between the feed and permeate side,[5−7] which could take full advantage of the solar, geothermal energy, and industrial waste heat,[8−10] wherein direct contact membrane distillation (DCMD) is the most popular and simplest operation configuration.[6]

With regard to MD membrane, sufficient hydrophobicity, an appropriate mean flow pore size (MFP), and a narrow pore size distribution could obtain a high liquid entry pressure of water (LEPw) to prevent membrane pores wetting.[11] Furthermore, microporosity and excellent breathability will play key roles in determining the osmotic transmission of volatile components (permeate vapor flux), while the mechanical property, thermal stability, and corrosion resistance of the membrane are also indispensable prerequisites for practical long-term MD operation.[6,12,13] Compared with traditional hydrophobic MD membrane with inner disconnected micorporous structures and poor porosity that is fabricated by phase inversion, stretching, sintering, or thermally induced phase separation,[14−17] a choreographed superhydrophobic electrospun nanofibrous membrane (ENM) exhibits a series of attractive characters, such

Received: July 18, 2015
Accepted: September 15, 2015
Published: September 15, 2015

DOI: 10.1021/acsami.5b06509
ACS Appl. Mater. Interfaces 2015, 7, 21919−21930

as a fully interconnected porous web structure, high porosity, and uniform fiber morphology with controllable pore size and membrane thickness, etc.,[18−20] which could remarkably improve the drawback of low permeate vapor flux and avoid membrane pores wetting efficiently during the MD process.

Since the first report of electrospun PVDF nanofibrous membrane for air-gap MD to produce potable water by Feng et al.[21] in 2008, various approaches have been implemented for the fabrication of PVDF[22,23] and modified PVDF ENMs[24−30] to augment the permeability and selectivity of MD performance, such as the hot-press posttreatment of PVDF nanofiber membrane,[22] PVDF blended with clay nanocomposites,[24] poly(vinylidene fluoride)-*co*-hexafluoropropylene (PVDF-HFP) and nanocrystalline cellulose reinforced PVDF-HFP,[25,26] and superhydrophobic modified PVDF ENMs, etc.[27−30] Nevertheless, these membranes still exhibited a limited enhancement of permeate vapor flux in the MD process, even though the well designed dual-layer or triple-layer hydrophilic−hydrophobic composite nanofibrous membranes[31,32] and the exploitation of novel electrospun poly(tetrafluoroethylene) (PTFE) and polyamide nanofibers.[33,34] Maab et al.[35] have demonstrated the fabrication of electrospun aromatic fluorinated polyoxadiazoles (F-POD) and polytriazoles (F-PT) nanofibrous membranes with considerable permeate vapor flux of about 40 kg/(m^2·h) at a temperature difference of 38 °C under the real seawater feed solution; while the continuous DCMD test was just carried out for 1 h, the long-term stability of MD performance needs to be further considered. It is noteworthy that the pore size distribution of an electrospun nonwoven layer structure is correlated with the fiber diameter and the bulk porosity;[36] i.e., the larger average fiber diameter will result in the larger mean flow pore size (MFP) and vice versa, which will directly determine the change of permeate vapor flux under the same surface wettability. Thus, it is of vital importance to discuss the relationship between fiber diameter distribution and MFP in detail. Previously, we have demonstrated a new type of dual-biomimetic polystyrene (PS) superhydrophobic membrane with microfibers and nanofibers that exhibited a competitive permeate vapor flux over 10 h of testing,[37] in spite of the thermal stability, corrosion resistance, and mechanical rigidity of the membrane maybe of limited duration.

Colloid electrospinning, a significant variant of the electrospinning technique, has recently emerged in popularity,[38] which could provide a simple strategy to construct superhydrophobic organic/inorganic composite nanofibers with hierarchical structures by electrospinning the functional inorganic colloidal nanoparticle/polymer matrix.[39,40] Benefiting from the accessible functionalization of silica nanoparticles and the electrospinning instability of PVDF matrix, various micro-/nanoscaled roughnesses could be formed on the PVDF nanofiber surfaces and exhibited different delicate nanofiber morphology and fiber diameter distribution, which will play a key role in the augmentation of permeate vapor flux. Herein, we describe a novel electrospun superhydrophobic organic/inorganic composite nanofibrous membrane with prominent MD performance fabricated by a facile route combining the hydrophobization of SiO_2 NPs and colloid electrospinning of the hydrophobic silica/PVDF matrix (as shown in Scheme 1). Significantly, the obtained superhydrophobic membrane with excellent structural attributes could be applied for desalination via DCMD and exhibited a remarkable potable water productivity triggered by regulating an optimized MFP from the different fiber diameter distribution.

Scheme 1. Illustration for the Fabrication Procedure of Electrospun Superhydrophobic Organic/Inorganic Composite Nanofibrous Membranes for Direct Contact Membrane Distillation

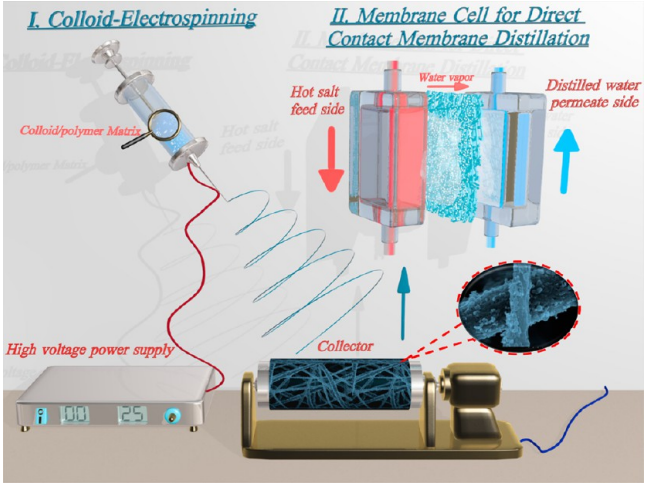

EXPERIMENTAL SECTION

Materials. Commercial polymer PVDF (with weight-average molecular weight of 573000 g/mol) was purchased directly from Solvay Shanghai Co., Ltd. *N*,*N*′-Dimethylformamide (DMF), toluene, isopropyl alcohol (IPA), tetraethyl orthosilicate (TEOS; was used as a sol−gel precursor to synthesize silica particles), ammonia solution ($NH_3·H_2O$, 28%), absolute ethanol, methyl blue, direct red, methyl orange, and Sunset Yellow FCF (SY FCF) were kindly supplied by Shanghai Lingfeng Chemical Reagent Co., Ltd. (China). Octadecyltrichlorosilane ($CH_3(CH_2)_{16}CH_2SiCl_3$, OTS), for the silica surface modification, was purchased from Sigma-Aldrich. All chemicals were of analytical grade and were used as received without further purification. Commercial PVDF membranes with mean pore size of 0.22 μm were utilized to compare with the functional PVDF nanofibrous membranes fabricated in this study.

Preparation of Hydrophobic Silica Colloidal Dispersions. Monodisperse silica nanoparticles (SiO_2 NPs) with three different sizes of 40, 167, and 210 nm were synthesized by the Stöber−Fink−Bohn method[41] and a modified seeded-growth procedure[42] (preparation details have been described in the Supporting Information). To improve the dispersion of SiO_2 NPs in the PVDF matrix efficiently and avoid the nanoparticles agglomeration and the hydrophilic component in the membrane matrix eventually, the hydrophobization of SiO_2 NPs is necessary to allow their dispersions in nonaqueous solvents.[43] While silane coupling agents are the most used type of decoration reagents, for instance, OTS is utilized in this study. Briefly, 1 g of SiO_2 NPs and 100 mL of toluene were mixed together in a 250 mL three-neck round-bottom flask equipped with a condenser. The mixture was homogenized via ultrasonic treatment for 1 h and stirred at 400 rpm in an oil bath with room temperature for 30 min; then 2 mL of OTS diluted with 8 mL of toluene was added into the flask, and the reaction was allowed to proceed at 112 °C for 24 h. The resultant OTS−silica nanoparticles were centrifuged and washed thrice in sequence with toluene and absolute ethanol. Finally, the obtained particles were dried at 80 °C under vacuum for 24 h and re-dispersed in DMF to form colloidal suspensions.

Colloid-Electrospinning Details. Typically, PVDF was dissolved in DMF by mild stirring in an oil bath (~70 °C) for 48 h to obtain an 18 wt % homogeneous transparent solution. Then, 20 wt % OTS−silica/DMF suspensions with particle sizes of 167 and 210 nm were mixed with 18 wt % PVDF/DMF solution in a weight ratio of 1:2, respectively. In consideration of the SiO_2 NPs with the smallest size of 40 nm, a mixture of 30 wt % OTS−silica/DMF suspension and 18 wt % PVDF/DMF solution with a weight ratio of 1:2 was utilized to form the OTS−silica/PVDF dispersions. These mixtures of colloids and PVDF were

DOI: 10.1021/acsami.5b06509
ACS Appl. Mater. Interfaces 2015, 7, 21919−21930

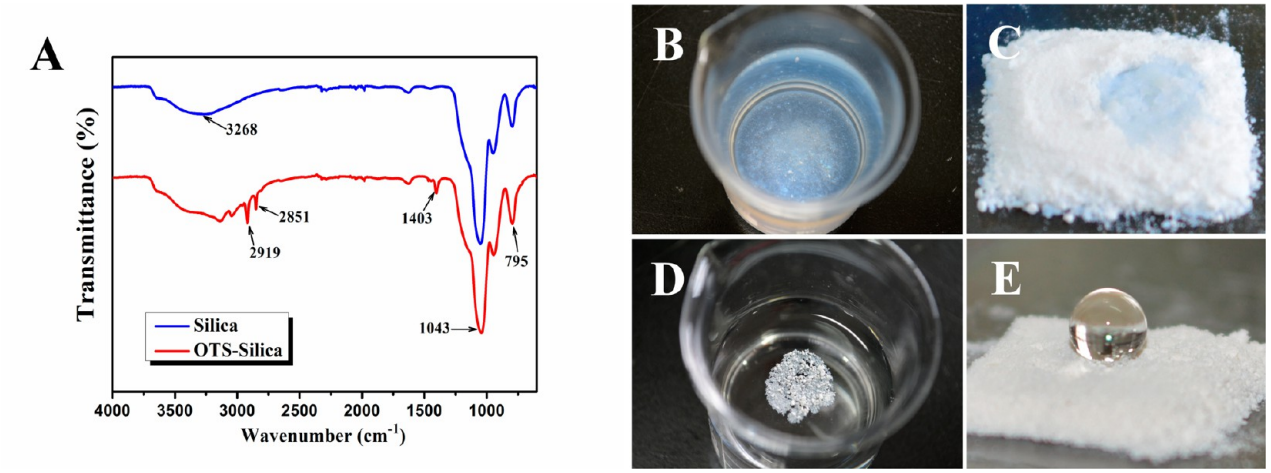

Figure 1. (A) FT-IR spectra of silica and OTS−silica. Photographic images of surface wettability of silica (B, C) and OTS−silica (D, E).

homogenized via vigorous stirring in an oil bath at 60 °C for 24 h and ultrasonic treatment for 2 h prior to the electrospinning process.

About 5 mL of the OTS−silica/PVDF dispersion was placed in a 5 mL syringe equipped with a blunt metal needle of 0.37 mm inner diameter. The syringe was placed in a syringe pump that maintained a solution feeding rate of 5 μL/min. A grounded metallic rotating roller covered with a piece of aluminum foil was used as collector, which rotated at 500 rpm. The distance between the needle tip and collector was 15 cm, and the voltage was set at 25 kV. The relevant temperature and humidity were 30 ± 2 °C and 30 ± 5%, respectively. The obtained electrospun nanofibrous scaffolds were dried in a vacuum oven at 60 °C for 12 h to remove the residual solvent and denoted as PVDF-S-*x* (where *x* stands for the different silica particle sizes). Meanwhile, PVDF ENM was also prepared by the same electrospinning circumstance. The resultant membranes were cold-pressed at room temperature under 2 MPa pressure for 30 s to improve their dimensional integrity with the same membrane thickness of 100 μm.

Characterizations of Electrospun Composite Nanofibrous Membranes. The surface morphology of the silica nanoparticles and electrospun nanofibrous membranes were investigated by field emission scanning electron microscopy (FE-SEM, SU8000, Hitachi, Tokyo, Japan) and transmission electron microscopy (TEM, JEM-2100, JEOL, Tokyo, Japan). The surface chemical compositions of the samples were measured by a Nicolet 8700 FT-IR spectrometer in the range of 650−4000 cm^{-1} (attenuated total reflectance mode, Thermometer, USA). SiO_2 NPs sizes and fiber diameters together with their distribution were measured using an image analyzer, namely, ImageJ 2X software; 5 SEM images have been considered, and the sizes of a total number of 200 particles have been measured as well as the diameters of a total number of 200 fibers. The wettability of the surface was performed by a dynamic contact angle testing instrument (OCA40, Dataphysics, Filderstadt, Germany) equipped with a dynamic image capture camera. Average water contact angles were obtained by measuring the same sample at five different positions.

The Brunauer−Emmett−Teller (BET) surface area of the electrospun sample was characterized by using N_2 adsorption−desorption isotherms with an ASAP 2020 physisorption analyzer (Micromeritics Co., Norcross, GA, USA). The mean flow pore size (MFP), pore size distribution, bubble point, or maximum pore size of the as-prepared membranes were characterized by using a capillary flow porometer (CFP-1100A, Porous Material. Inc. (PMI)) based on the wet/dry flow method, where the membranes were initially wetted with wetting liquid (perfluoroether, Porefil) and subsequently placed in a sealed chamber through which gas flows. The change in flow rate was measured as a function of pressure for both dry and wet processes. And the results were obtained by the following equation:[44]

$$P = \frac{4\gamma \cos\theta}{D}$$

where P is the differential pressure, γ is the surface tension of the wetting liquid, θ is the contact angle of the wetting liquid (in this case zero), and D is the pore diameter. The gas flow rate measured through dry membranes yielded the gas permeability.[44] According to Darcy's law, the flow of fluids through porous media was proportional to the pressure gradient causing flow.[45]

The mechanical properties of the resultant membranes were measured on a tensile testing machine (WDW3020, Changchun Kexin, China). The porosity of the membrane is defined as the volume of the pores divided by the total volume of the membrane, which can be determined by a gravimetric method (described in the Supporting Information).[46] The liquid entry pressure of water (LEPw) is commonly characterized as the ability of the membrane to hinder any liquid water penetrating into membrane pores,[46] which could be used to assess the antiwetting capability of the as-prepared samples. A homemade experimental apparatus schematized in the Supporting Information (Figure S2) was used for LEPw measurements.

Direct Contact Membrane Distillation Performance. A 0.22 μm commercial PVDF membrane (mean pore size 0.22 μm) and PVDF and PVDF-S-*x* ENMs were applied to the DCMD test with an effective membrane area of 30 cm^2. The schematic diagram of the DCMD experimental setup (see the Supporting Information, Figure S3) has been detailed in our previous work.[37] In this study, the DCMD test was conducted with 3.5 wt % NaCl aqueous solution as feed, and the permeate tank was distilled water (a conductivity of around 2.45 μs/cm). The feed temperature was heated to 60 °C by one heating system and circulated with a flow rate of 0.6 L/min by a diaphragm laboratory pump, while the permeate side was maintained at 20 °C by one chiller to condense the permeate vapors and circulated by another diaphragm laboratory pump at the same flow rate. During the test, the conductivity of the permeate solution was monitored by conductivity meters (SevenEasy, Mettler Toledo) and the permeate vapor flux was obtained by the weight increase of the permeate tank which was located on one digital balance (MS6001S, Mettler Toledo).

RESULTS AND DISCUSSION

Surface Morphology and Surface Property. Utilization of inorganic nanoparticles for creating functional surfaces has gained substantial attention; particularly, silica nanoparticles (SiO_2 NPs) have been frequently applied for the construction of superhydrophobic and superhydrophilic surfaces with hierarchical roughness.[47] By a facile combination of the Stöber−Fink−Bohn method and a modified seeded-growth procedure,[41,42] monodisperse SiO_2 NPs with different size and a narrow size distribution could be conveniently manipulated by varying the reaction components (reactants, catalyst, and solvent) and circumstance. The representative FE-SEM images of the as-

DOI: 10.1021/acsami.5b06509
ACS Appl. Mater. Interfaces 2015, 7, 21919−21930

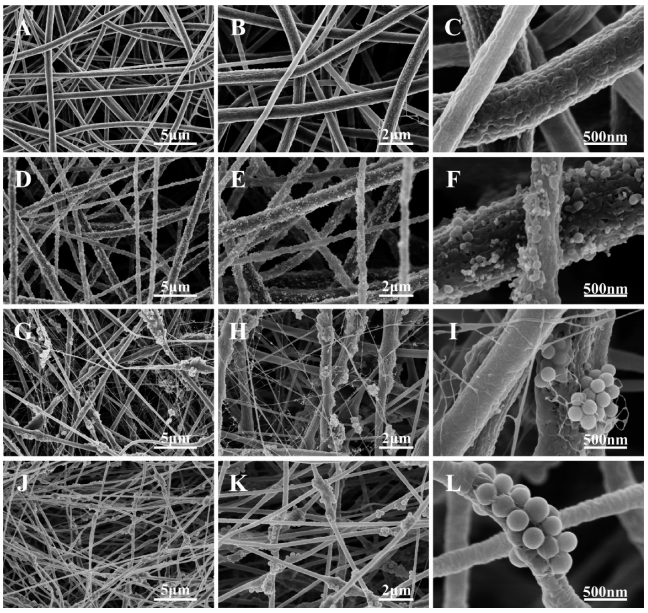

Figure 2. FE-SEM images of electrospun nanofibrous membranes (A–C) PVDF, (D–F) PVDF-S-40, (G–I) PVDF-S-167, and (J–L) PVDF-S-210.

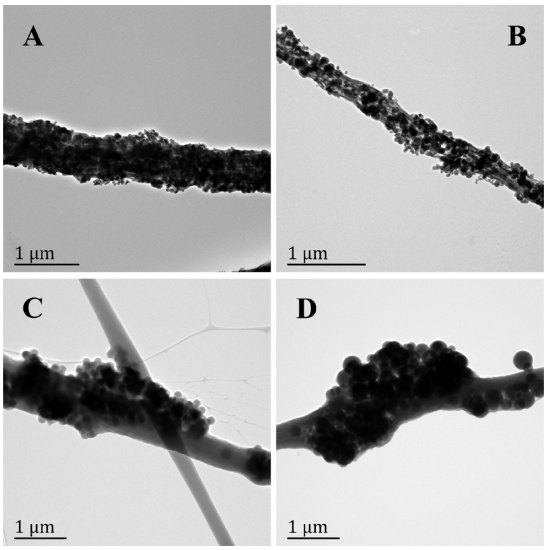

Figure 4. Representative TEM images of (A, B) PVDF-S-40, (C) PVDF-S-167, and (D) PVDF-S-210 ENMs.

synthesized SiO_2 NPs were shown in Figure S1, which exhibited smooth spherical morphology, uniform in particle size and narrow size distribution; i.e., these obtained SiO_2 NPs possess good monodispersity. Three different SiO_2 NPs with 40, 167, and 210 nm were applied to investigate the effect of particle size on nanofiber morphology, fiber diameter distribution, surface wettability, membrane structural attributes and DCMD performances.

It is noteworthy that an increase in hydrophobicity of the SiO_2 NPs will be beneficial to the filler/matrix miscibility, and an improvement of interfacial interaction could be yielded by the molecular entanglement between the hydrophobic grafting chains on the modified SiO_2 NPs surface and the matrix

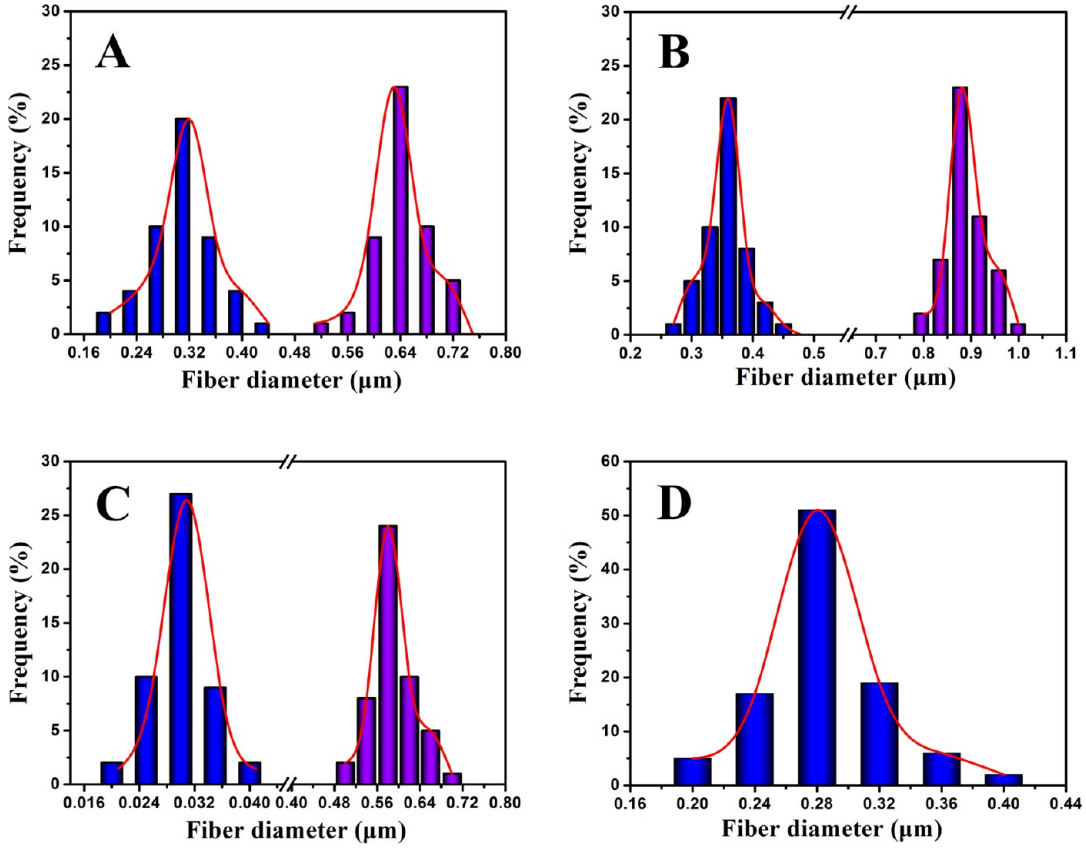

Figure 3. Fiber diameter distribution of (A) PVDF, (B) PVDF-S-40, (C) PVDF-S-167, and (D) PVDF-S-210 ENMs.

DOI: 10.1021/acsami.5b06509
ACS Appl. Mater. Interfaces 2015, 7, 21919–21930

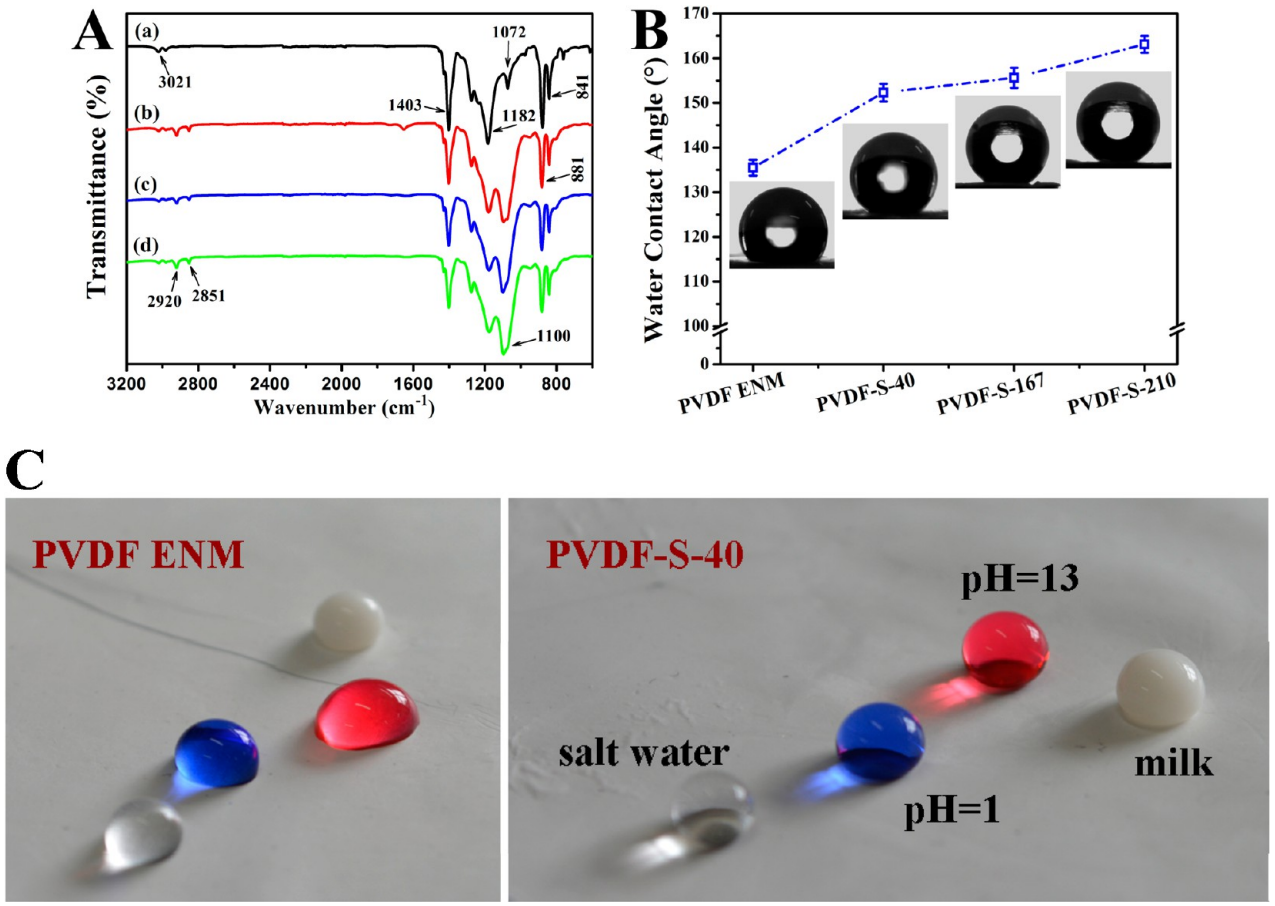

Figure 5. (A) FT-IR spectra of (a) PVDF, (b) PVDF-S-40, (c) PVDF-S-167, and (d) PVDF-S-210 membranes. (B) Water contact angles variation from the membranes with different silica particles sizes. (C) Photographic images of droplets of salt water, acidic water (dyed with methyl blue), alkaline water (dyed with direct red) and milk on the surfaces of PVDF and PVDF-S-40.

polymer.[43] Thus, in order to improve the dispersion of SiO_2 NPs in the PVDF matrix efficiently and avoid the nanoparticles agglomeration and the hydrophilic component in the membrane matrix eventually, the hydrophobization of SiO_2 NPs with OTS was carried out in this study. The graft of OTS on SiO_2 NPs surfaces could be confirmed from FT-IR spectral analysis, as shown in Figure 1A; the strong broad peaks around 3268 cm^{-1} (OH stretching vibration), 1043 cm^{-1} (Si−O−Si stretching), and 795 cm^{-1} (Si−O stretching) were assigned to hydrophilic silica nanoparticles, and an exhibition of three new absorption bands with peaks at 2919, 2851, and 1403 cm^{-1}, which corresponds to the CH_2 stretching and wagging vibration, indicated the grafting of OTS on SiO_2 NPs surfaces successfully. Additionally, the surface wettability of silica and OTS−silica nanoparticles were investigated by sprinkling them into the water and observing the state of water droplets on the rough SiO_2 NPs stack surfaces. As shown in Figure 1B−E, the hydrophilic silica could be dispersed in water and the water droplet could be spread into the stack rapidly. In contrast, the OTS−silica nanoparticles were floated on the water surface and a spherical water droplet could be located on the stack surface and even exhibited a superhydrophobic surface wettability, which further proved the introduction of OTS onto the surface of SiO_2 NPs.

Inspired by the special wettability of biological organisms from nature, the cooperation of their unique micro-/nanoscaled surface structures and low surface energy is thought to be the contributing factor for the superhydrophobicity. Nevertheless, a hierarchical structure is commonly recognized as the strategic factor for superhydrophobization due to the air pockets to be entrapped underneath the water droplet as a repulsive cushion.[48,49] Herein, an appropriate multiscaled roughness was successfully textured through the immobilization of the SiO_2 NPs on the PVDF nanofibers surfaces. The representative FE-SEM images of as-prepared PVDF and PVDF-S-*x* ENMs shown in Figure 2A−L exhibited randomly oriented 3D nonwoven scaffolds with various surface morphology. As can be seen from Figure 2A−C, a typically rough PVDF nanofiber with micro-grooves along the fiber axis was introduced by constructing microwrinkles on the nanofiber surface, and these unique surface topographies could be explained by the buckling instabilities associated with the solvent evaporation from the surface of the fluid jet and trapped inside the jet which resulted in a contraction mismatch.[50] Meanwhile, the existence of PVDF nanofibers with two different average fiber diameters of about 320 and 630 nm (as shown in Figure 3A) resulted from the axially symmetric instability in the process of spin charged jet bending and stretching.[51] By introducing the OTS−silica colloids in the PVDF matrix, the low surface energy of long alkyl chain and polymer chain will competitively move to the surface of nanofibers during the fast phase separation process in electrospinning,[52] and the hydrophobic SiO_2 NPs were inclined to transfer from the core to shell of the PVDF nanofibers when using a low vapor pressure solvent of DMF.[53] As shown in Figure 2D−L, various hierarchical roughness containing microwrinkles and nanoprotrusions were successfully constructed on the PVDF nanofiber surfaces. In the case of silica nanoparticles size with 40

DOI: 10.1021/acsami.5b06509
ACS Appl. Mater. Interfaces 2015, 7, 21919−21930

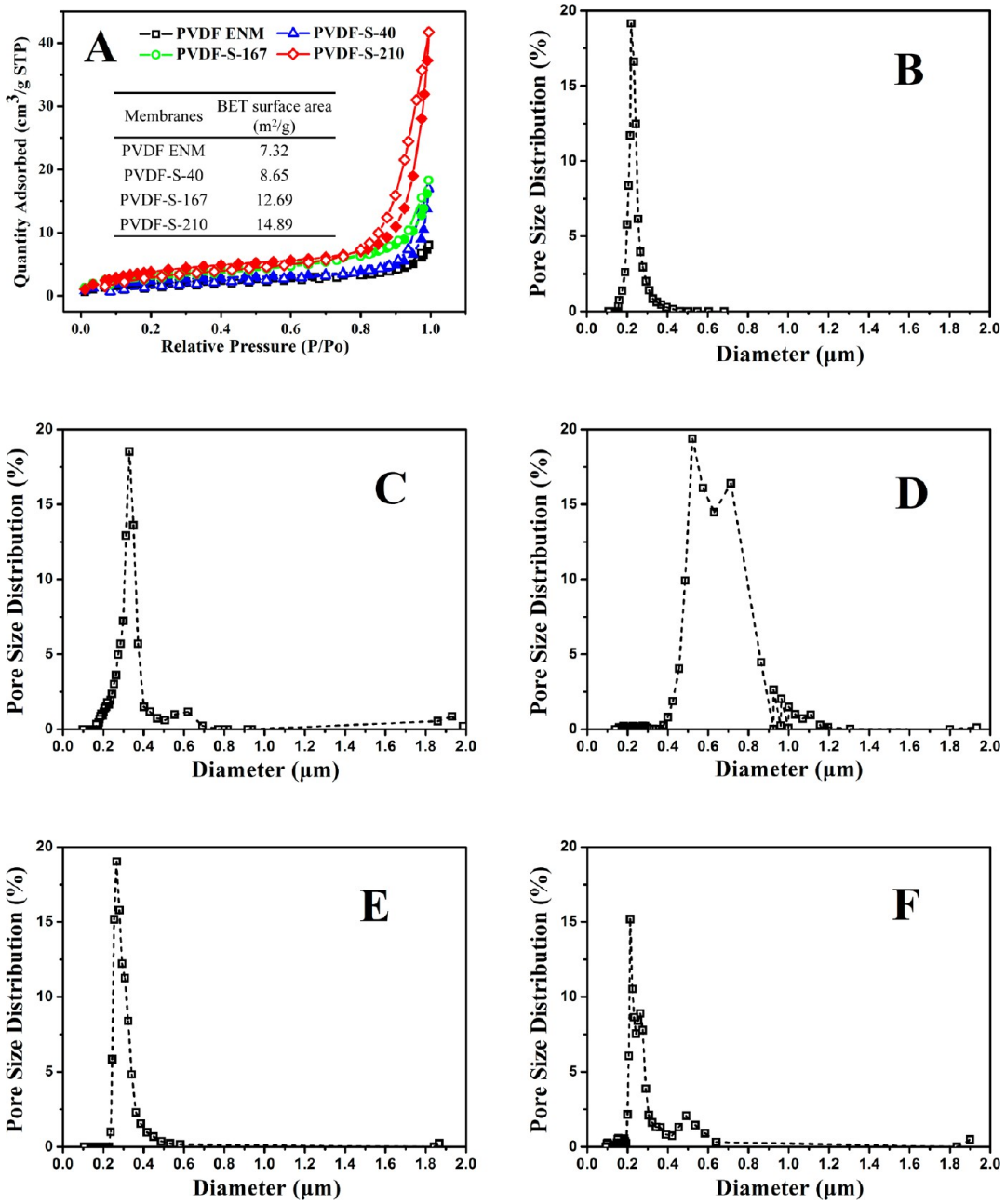

Figure 6. (A) N_2 adsorption−desorption isotherms of PVDF, PVDF-S-40, PVDF-S-167, and PVDF-S-210 ENMs. Pore size distribution of (B) commercial PVDF membrane and (C) PVDF, (D) PVDF-S-40, (E) PVDF-S-167, and (F) PVDF-S-210 ENMs.

Table 1. Structural Attributes of Commercial PVDF Membrane and PVDF and PVDF-S-*x* ENMs

membranes	pore size range (μm)	MFP size (μm)	porosity (%)	LEPw (bar)
0.22 μ PVDF	0.1568−0.6816	0.2203	56.1 ± 2.0	2.35 ± 0.05
PVDF ENM	0.1815−1.9855	0.3233	80.4 ± 1.5	1.20 ± 0.10
PVDF-S-40	0.2190−1.9339	0.6110	79.7 ± 2.2	1.65 ± 0.05
PVDF-S-167	0.2442−1.8671	0.2868	76.2 ± 1.3	2.20 ± 0.15
PVDF-S-210	0.1479−1.9003	0.2429	69.0 ± 1.5	2.40 ± 0.10

nm, electrospun PVDF-S-40 nanofibers exhibited a similar phenomenon with PVDF sample that contained two different average fiber diameters with about 360 and 880 nm (as shown in Figure 3B). It is noteworthy that PVDF-S-40 showed a good distribution of hydrophobic SiO_2 NPs on the nanofiber surfaces without obvious agglomeration, which could be confirmed by the representative TEM images, as shown in Figure 4A,B, both of the fibers with two different diameters were compact enveloped by uniform SiO_2 NPs. Nevertheless, with the increase of silica particle sizes to 167 and 210 nm, the agglomeration state of SiO_2 NPs was partially formed along the nanofiber axis, even the PVDF-S-210 sample exhibited a pea-like morphology. As can be seen from Figure 4C,D, the functional SiO_2 NPs were inclined to transfer from the core to shell of the PVDF nanofibers when

DOI: 10.1021/acsami.5b06509
ACS Appl. Mater. Interfaces 2015, 7, 21919−21930

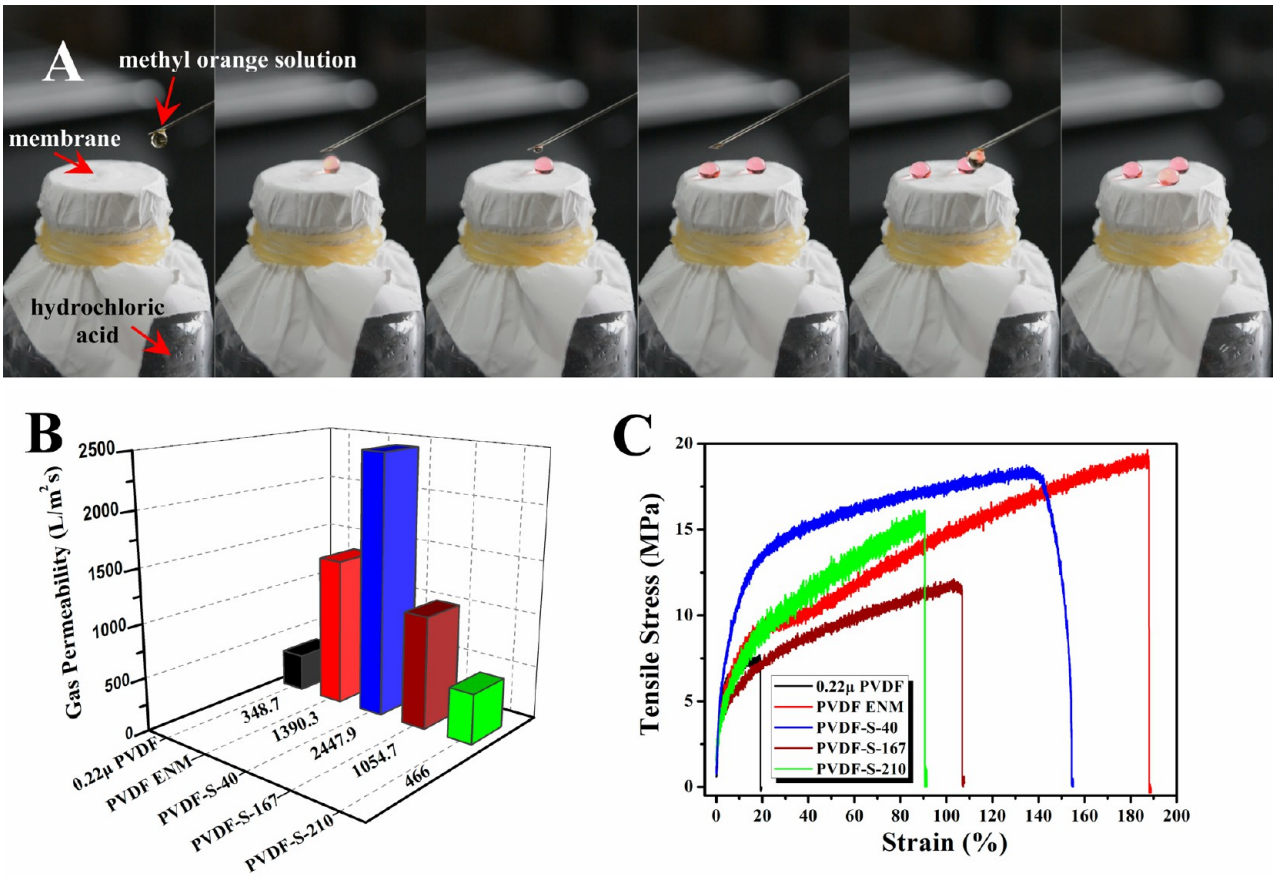

Figure 7. (A) Breathable performance of PVDF-S-40 ENM by using a methyl orange pH indicator solution and hydrochloric acid as a volatile solution. (B) Gas permeability results and (C) tensile stress−strain curves of the commercial PVDF membrane and PVDF and PVDF-S-*x* ENMs.

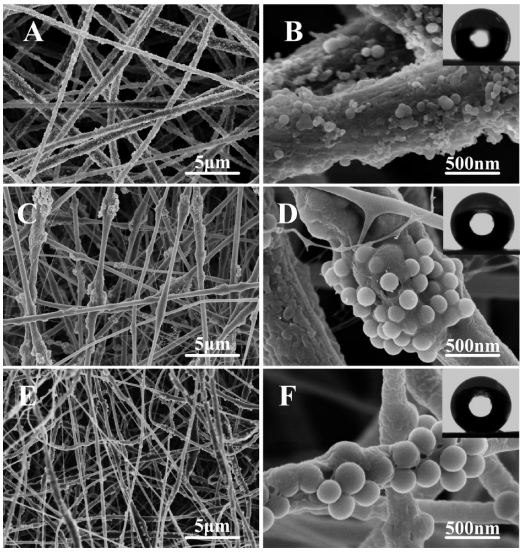

Figure 8. FE-SEM images of (A, B) PVDF-S-40, (C, D) PVDF-S-167, and (E, F) PVDF-S-210 ENMs after ultrasonication in IPA for 1 h with 80 °C circumstance. The insets in panels B, D, and F are the water contact angles.

utilizing the DMF circumstance. More importantly, there were no obvious SiO_2 NPs aggregation electrosprayed on the 3D electrospun nonwoven scaffolds. On the other hand, the average fiber diameters of PVDF-S-167 and PVDF-S-210 were remarkably changed, as shown in Figure 2G−L and Figure

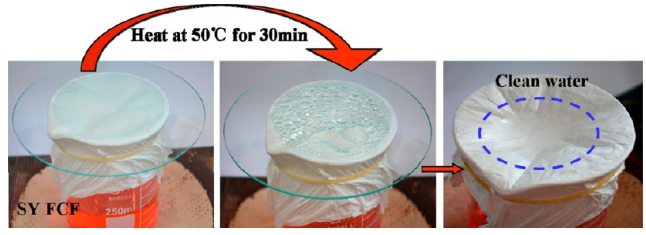

Figure 9. Schematic diagram for the simulation of the MD process with PVDF-S-40 ENM.

3C,D, PVDF-S-167 exhibited a nanofiber (~580 nm)/ultrafine nanofiber (~30 nm) composite structure, which could be ascribed to the occurrence of second electrospinning among the adjacent nanofibers and/or silica nanoparticles due to the inorganic nanoparticles could contain higher electronic density than polymer templates in the electrospinning process.[38] Nevertheless, PVDF-S-210 showed uniform nanofiber (~280 nm) morphology that may result from the larger particle size and the relative decrease of solution viscosity. Consequently, the combination of PVDF nanofibers with immobilized SiO_2 NPs constructed the surface hierarchical roughness.

FT-IR spectral analysis was employed to confirm the surface chemical compositions of PVDF and PVDF-S-*x* ENMs; as shown in Figure 5A, the peaks around 3021 cm^{-1} (CH_2 stretching vibration), 1403 cm^{-1} (CH_2 wagging), 1182 cm^{-1} (CF_2 stretching), 881 cm^{-1} (C−C skeleton vibration), and 1072 and 841 cm^{-1} (crystal phase vibration) were observed for the PVDF sample, whereas PVDF-S-*x* ENMs exhibited a new strong

DOI: 10.1021/acsami.5b06509
ACS Appl. Mater. Interfaces 2015, 7, 21919−21930

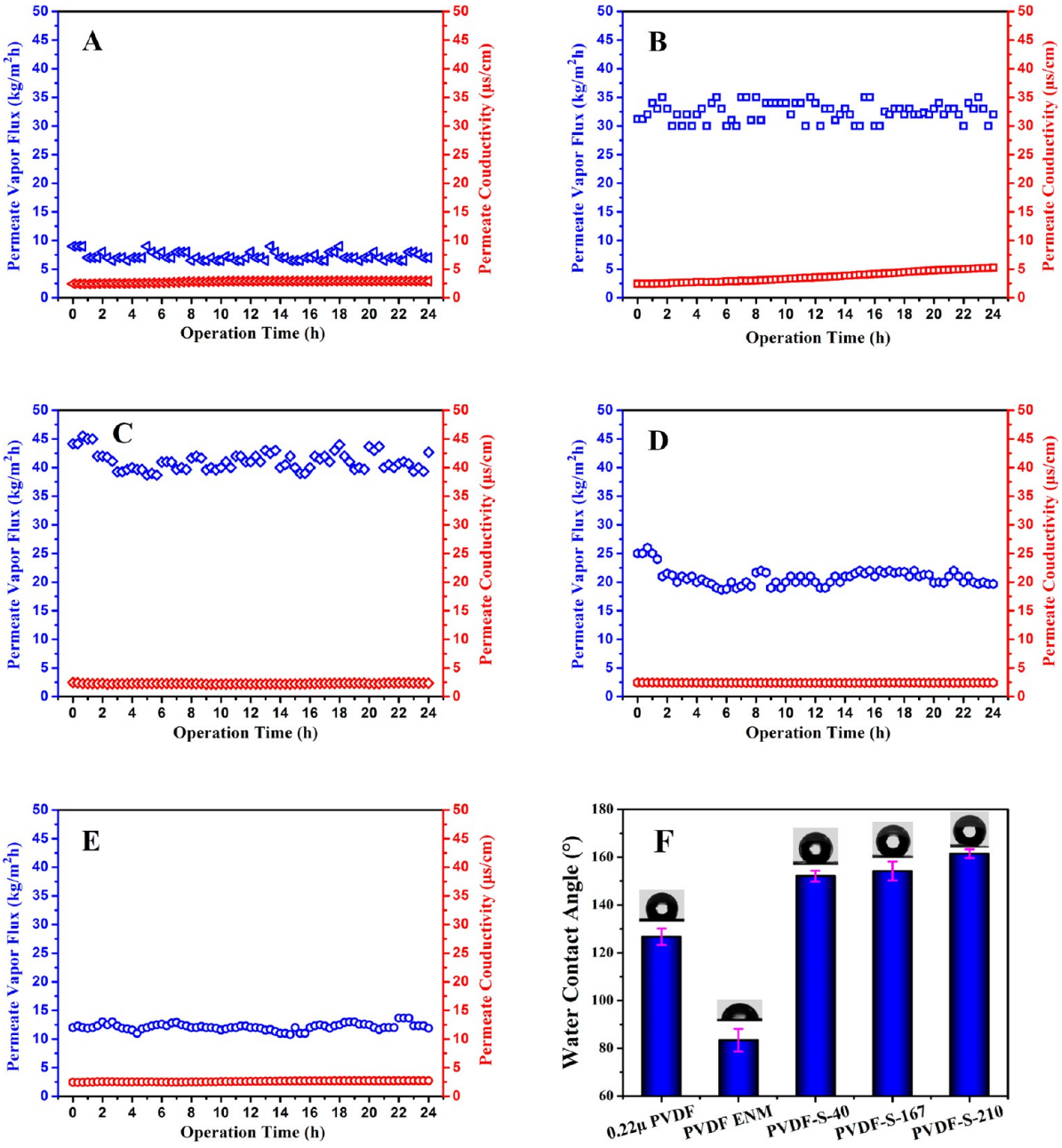

Figure 10. Continuous DCMD test of (A) commercial PVDF membrane and (B) PVDF, (C) PVDF-S-40, (D) PVDF-S-167, and (E) PVDF-S-210 ENMs (3.5 wt % NaCl solution as feed; ΔT = 40 °C; flow rate at feed and permeate side = 0.6 L/min). (F) Water contact angles of the membranes after DCMD test.

broad band with the peak at 1100 cm^{-1}, which corresponds to the Si−O−Si stretching vibration. Meanwhile, the peaks that appeared at 2920 and 2851 cm^{-1} were assigned to the CH_2 stretching vibration of OTS−silica. Thus, the FT-IR information fully confirmed the construction of multiscaled PVDF-S-*x* ENMs successfully. It is noteworthy that the resultant PVDF-S-*x* nanofibers with hierarchical roughness containing microwrinkles and nanoprotrusions would lead to the decrease in the air fraction of solid/liquid interfaces beneath the water droplet by reducing the actual contact area of the water droplet on the surface structures, and finally resulting in boosting the hydrophobicity of membranes; as shown in Figure 5B, the water contact angles (WCAs) of PVDF, PVDF-S-40, PVDF-S-167, and PVDF-S-210 ENMs were 135.5 ± 1.8°, 152.3 ± 2.0°, 155.6 ± 2.3°, and 163.1 ± 1.9°, respectively, indicating a remarkable increment of WCA toward the increasing silica nanoparticles sizes due to the surface geometry effect,[54] wherein the salt water, acidic water (pH = 1), alkaline water (pH = 13), and milk droplets with about 10 μL will spread with small contact angles on the PVDF ENM surface, whereas all of them could be located on the PVDF-S-40 surface with high contact angles that exceed 150°, indicating the insufficient surface roughness of PVDF and the certain stability against corrosive conditions. The prominent enhancement of hydrophobicity of PVDF-S-*x* could be further confirmed by investigating the Brunauer−Emmett−Teller (BET) surface areas of membranes; as shown in Figure 6A, the resultant electrospun nanofibrous membranes exhibited the isotherm of type IV according to the International Union of Pure and Applied Chemistry (IUPAC) classification.[55] The BET surface areas of PVDF, PVDF-S-40, PVDF-S-167, and PVDF-S-

DOI: 10.1021/acsami.5b06509
ACS Appl. Mater. Interfaces 2015, 7, 21919−21930

Table 2. Properties and DCMD Performances of Different Modified PVDF ENMs

membrane	WCA (deg)	MFP size (μm)	porosity (%)	LEPw (bar)	membrane thickness (μm)	feed side		permeate side		permeate vapor flux (kg/(m^2·h))	rejection (%)	stable in long-term operation
						solution	T_f (°C)	solution	T_p (°C)			
PVDF-clay ENMs[24]	154.2	0.64	81	2.0	300	3.5 wt % NaCl	80	deionized water	17	5.75	99.97	8 h tested
PVDF-HFP ENMs[25]	125.0	0.26	58	1.30	110	1.0 wt % NaCl	65	tap water (110 μs/cm)	24	20–22	98	
NCC reinforced PVDF-HFP ENMs[26]	132.2	0.20	75	1.90	225	1.0 wt % NaCl	60	tap water (180 μs/cm)	38	10.2	99	
PVDF–PDA-Ag-thiol ENMs[27]	153.0	0.34	77	1.46	47	3.5 wt % NaCl	60	distilled water	20	31.6	>99.99	8 h tested
PVDF-Silica electrospun composite membranes L-PVDF[29]	153.9	0.77	83	1.79	129	3.5 wt % NaCl	60	distilled water	20	18.9	>99.99	50 h tested
3S-N[30]	154.0	0.32	80	1.80	72	3.5 wt % NaCl	60	distilled water	20	24.6	>99.99	in 25 h
this study PVDF-S-40	152.3	0.61	79.7	1.65	100	3.5 wt % NaCl	60	distilled water	20	41.1	>99.99	24 h tested
PVDF-S-167	155.6	0.29	76.2	2.20	100	3.5 wt % NaCl	60	distilled water	20	20.8	>99.99	24 h tested

210 ENMs were 7.32, 8.65, 12.69, and 14.89 m^2/g, respectively, revealing an obvious increase in BET surface area with the increment of silica nanoparticles sizes. This could be attributed to the different hierarchical structures constructed by electrospinning OTS−silica/PVDF dispersions with different particles sizes; i.e., the surface roughness of ENMs exhibited an increscent tendency toward the increasing particle sizes, which was in accordance with the WCAs tested. Therefore, the promising superhydrophobicity could make PVDF-S-x ENMs good candidates for membrane distillation (MD).

Structural Attributes of Membranes. The resultant electrospun nanofibrous membranes and 0.22 μm commercial PVDF membrane (mean pore size, 0.22 μm) were utilized to characterize their structural properties for the DCMD evaluation. The MFP, pore size distribution, gas permeability, porosity, and LEPw of the membranes were characterized comprehensively. In general, a novel nanofibrous membrane with high filtration efficiency was designed based on the principle that the pore size distribution of a nonwoven layer structure is correlated with the fiber diameter and the bulk porosity;[36] i.e., the larger fiber diameter will result in the larger pore size and vice versa. Importantly, an appropriate MFP and a narrow pore size distribution were suggested for the performance of MD membrane to prevent membrane pores wetting;[6] that is to say, an appropriate nanofiber diameter distribution should be adjusted to satisfy the pore size requirements for MD application and further to obtain a high efficient MD performance (permeability and selectivity). As can be seen from Figure 6B–F and Table 1, the commercial PVDF membrane contained a narrow distribution of pore diameter in the range of 0.16−0.68 μm with MFP of 0.22 μm. Nevertheless, the electrospun nanofibrous membrane generally showed a relatively broader pore size distribution, which ranged from 0.18 to 1.99 μm with MFP of 0.32 μm, from 0.22 to 1.93 μm with MFP of 0.61 μm, from 0.24 to 1.87 μm with MFP of 0.29 μm, and from 0.15 to 1.90 μm with MFP of 0.24 μm, corresponding to the PVDF, PVDF-S-40, PVDF-S-167, and PVDF-S-210 ENMs, respectively. The PVDF-S-x sample exhibited a reduced tendency of MFP value toward the increment of silica particle sizes, which could be ascribed to the remarkable decrease of fiber diameter and the partially blocking result of SiO_2 NPs. As compared to PVDF ENM, the MFP of PVDF-S-40 was still larger than that of PVDF due to its larger fiber diameter, indicating the correlation between pore size and fiber diameter that was in accordance with the preceding FE-SEM analysis.

It is generally agreed upon that higher membrane bulk porosity will result in higher permeate vapor flux, and the MD membrane porosity could be ranged from 30 to 85% as reported so far.[10] As can be seen from Table 1, the commercial PVDF membrane exhibited the lowest porosity of 56.1 ± 2.0% compared with the as-prepared electrospun nanofibrous membranes. Although the partially blocking result of SiO_2 NPs will lead to the decrease of porosity, the PVDF and PVDF-S-x ENMs still have reasonably high porosity required for MD application, which was 80.4 ± 1.5, 79.7 ± 2.2, 76.2 ± 1.3, and 69.0 ± 1.5%, respectively.

LEPw (sometimes faultily called "wetting pressure") is the pressure that must be applied onto deionized water before it penetrates into a nonwetted (dry) membrane;[46] i.e., a water droplet cannot pass through the membrane below this breakthrough pressure, which is one of the crucial structural characteristics to guarantee the stability of membrane performance during the long-term MD operation. As compared to the commercial PVDF membrane with a high LEPw value of 2.35 ±

DOI: 10.1021/acsami.5b06509
ACS Appl. Mater. Interfaces 2015, 7, 21919−21930

0.05 bar due to its smallest MFP and narrowest pore size distribution, the electrospun nanofibrous membrane generally exhibited a relatively lower LEPw value.[22,24,25,35] However, a desired LEPw of membrane depends not only on the pore size, but on the membrane hydrophobicity and porosity. Thus, with the enhancement of water contact angles, the LEPw of PVDF and PVDF-S-*x* ENMs exhibited a remarkably increased tendency, as shown in Table 1, which was 1.20 ± 0.10, 1.65 ± 0.05, 2.20 ± 0.15, and 2.40 ± 0.10 bar, respectively. The maximum LEPw of PVDF-S-210 even exceeded that of conventional PVDF commercial membrane fabricated by phase inversion, which provided the basic structural prerequisite for MD application.

The fully interconnected porous structure of electrospun nanofibrous membrane would play a key role as the passageway for the transmission of water vapors, which performs as the breathability of the membrane. In the DCMD process, the permeate water vapors would be condensed into the cold fluid on the fluid−membrane interface by a circulated chiller system. Thus, the gas permeability of the resultant membranes is another crucial factor for estimating the permeate vapor flux across the membrane, which depends on the porosity, pore size, and membrane thickness, etc.[25] As stated previously, the gas permeability can be calculated from the gas flow rate through the dry membrane samples by using a capillary flow porometer. For the commercial PVDF membrane with mean pore size of 0.22 μm, as shown in Figure 7B, the gas permeability was 348.7 L/(m^2·s) at 20 psi because of its inner disconnected micorporous structures. Nevertheless, PVDF and PVDF-S-*x* ENMs contained outstanding values of gas permeability, which was 1390.3, 2447.9, 1054.7, and 466.0 L/(m^2·s) at 20 psi, respectively, and this tendency was in agreement with the preceding pore size analysis. Further study of breathable performance of PVDF-S-40 ENM was conducted by observing the color change of methyl orange pH indicator droplet (controlled by a microneedle to be about 10 μL) on a hydrochloric acid vial surface that was covered with the membrane. As can be seen from Figure 7A, the orange indicator droplet turned reddish immediately when the microneedle closed to the membrane surface (see the Supporting Information, Video), indicating the excellent breathability of PVDF-S-40 for the transmission of volatile hydrochloric acid gas.

Structural Stability of Membranes. In general, the mechanical properties of electrospun nanofibrous membranes were closely correlated with the intrinsic strength of the polymer nanofibers and the morphologic structure of nanofibers.[56] Figure 7C presented the typical tensile stress−strain curves of the resultant membranes. It is clearly showed that PVDF and PVDF-S-*x* ENMs exhibited a nonlinear elastic behavior during the initially external stress load because the relevant nonaligned nanofibers in 3D nonwoven scaffolds were forced to be aligned along the stress direction, and then exhibited a linear increase until the fracture of membranes due to the breakage of individual aligned nanofibers.[57] As compared to PVDF ENM, the elongation at the break of PVDF-S-*x* was reduced with the introduction of hydrophobic silica, which implied the relative brittleness of the OTS−silica/PVDF matrix. The obvious increase of tensile yield strengths of PVDF-S-40 and PVDF-S-210 could be also observed, which were attributed to the enhancement of surface roughness and different fiber diameter distribution, whereas PVDF-S-167 contained relatively lower tensile yield strength due to the existence of plenty of ultrafine fibers. Notably, all of these ENMs exhibited robust tensile strength (>10 MPa) and elongation at break (>90%) compared with the commercial PVDF membrane, indicating their good mechanical properties for MD application.

The robustness of the immobilized SiO_2 NPs was tested by ultrasonication in isopropyl alcohol for 1 h with 80 °C circumstance. The representative FE-SEM observations of as-prepared PVDF-S-*x* ENMs shown in Figure 8 demonstrated that hydrophobic SiO_2 NPs anchored on the PVDF nanofibers surfaces were able to withstand ultrasonication without significant decrease in coverage, which was ascribed to the sufficient molecular entanglement between the hydrophobic grafting chains on the modified SiO_2 NPs surface and the matrix polymer. Meanwhile, the membrane surface still exhibited a superhydrophobic property with a WCA of 152.1 ± 1.2°, 153.7 ± 2.0°, and 160.2 ± 2.1°, respectively, providing the basic structural prerequisite, thermal stability, and surface wettability for the long-term MD operation.

Direct Contact Membrane Distillation Performance. A schematic diagram shown in Figure 9 was utilized for the simulation of the MD process. It is clearly shown that clean water could be facilely obtained on the PVDF-S-40 ENM surface by heating the aqueous solution containing a nonvolatile component of Sunset Yellow FCF (SY FCF) at 50 °C for 30 min; i.e., the water vapors easily passed through the membrane and then condensed to water droplets on the inner wall of watch glass which could be collected by the membrane without penetration, indicating the straightforward illustration of the basic separation principle of MD.

The continuous DCMD tests of the 0.22 μm commercial PVDF membrane and PVDF and PVDF-S-*x* ENMs were performed over a period of 24 h operation by using a 3.5 wt % NaCl aqueous solution as the feed under a temperature of 60 °C, and the permeate side was maintained at 20 °C. As shown in Figure 10A−E, the conventional PVDF commercial membrane fabricated by phase inversion presented the lowest permeate vapor flux of 7.2 kg/(m^2·h) due to its inner disconnected micorporous structures, smallest mean flow pore size (MFP), narrowest pore size distribution, and poor porosity, whereas the high LEPw of the membrane remedied its insufficient hydrophobicity and guaranteed the stable low permeate conductivity (~2.45 μs/cm). As for PVDF electrospun nanofibrous membrane with completely interconnected porous structure, relatively larger MFP, and high porosity, the permeate vapor flux reached up to 32.5 kg/(m^2·h), fully demonstrating the excellent gas breathability of PVDF ENM. Unfortunately, the inadequate hydrophobicity of the membrane would finally result in the gradual increase of permeate conductivity after 10 h MD operation and exceeded 5 μs/cm within 24 h, indicating that the membrane pores suffered wetting, which could be further confirmed by the water contact angle (WCA, 83.4 ± 4.8°, as shown in Figure 10F) tested after MD operation. Interestingly, the choreographed superhydrophobic PVDF-S-40 ENM with hierarchical roughness containing microwrinkles and nanoprotrusions presented a prominent permeate vapor flux of 41.1 kg/(m^2·h) and stable low permeate conductivity (~2.45 μs/cm). This highly efficient desalination efficiency was ascribed to the largest MFP of PVDF-S-40 which resulted from the existence of two different average fiber diameters as analyzed previously, and the superhydrophobicity of the membrane guaranteed the production of high quality water. Meanwhile, PVDF-S-40 ENM still possessed a WCA of 152.1 ± 2.3° after 24 h MD testing, indicating the potential durability of the membrane for long-term operation. On the other hand, with the increment of silica particle sizes, the permeate vapor fluxes of PVDF-S-167 and

DOI: 10.1021/acsami.5b06509
ACS Appl. Mater. Interfaces 2015, 7, 21919−21930

PVDF-S-210 ENMs were gradually decreased due to the reduction of MFP and porosity, which were 20.8 and 12.2 kg/(m^2·h), respectively. In addition, the two membranes with outstanding LEPw also produced high quality water with stable low permeate conductivity (~2.45 μs/cm), and both of them contained the superhydrophobic property with WCAs of 154.2 ± 4.0° and 161.5 ± 1.9° after continuous MD process. Consequently, in order to obtain excellent desalination efficiency, the compromise could be made by constructing a superhydrophobic electrospun nanofibrous membrane with relatively larger MFP to ensure a desired LEPw for the stability of MD performance during the long-term operation. Furthermore, on the basis of a superhydrophobic property, how to design an appropriate electrospun fiber morphology with different fiber diameter distribution that could obtain different mean flow pore size for the excellent permeate vapor flux needs further investigation,[37] and the MD recyclability of PVDF-S-x ENMs will also be carried out in our future research.

Table 2 showed the comparison of properties and DCMD performances of different modified PVDF ENMs reported so far and the functional PVDF-S-*x* ENMs designed in this study. It could be concluded that a considerable enhancement of permeate vapor flux with long-term stability of PVDF-S-40 ENM has been achieved, which was primarily attributed to the superhydrophobic property, unique hierarchical structures and two different fiber diameter distributions in 3D nonwoven scaffolds, and this may be the most prominent difference compared with other modified PVDF ENMs. Therefore, the previously obtained stable MD performance (permeability and selectivity) suggested PVDF-S-*x* ENMs we demonstrated here could be used as a potential alternative for commercial MD membranes.

CONCLUSIONS

In summary, we have described the fabrication of novel superhydrophobic PVDF-S-*x* ENMs with excellent DCMD performance by colloid-electrospinning PVDF matrix blended with hydrophobic silica nanoparticles. The silica nanoparticle sizes have a decisive influence on the nanofiber morphology, fiber diameter distribution, surface wettability, and membrane structural attributes. The resultant PVDF-S-*x* ENMs with high porosity, considerable LEPw values, fabulous gas permeability, excellent durability in ultrasonic treatment with 80 °C circumstance, remarkable mechanical properties and corrosion resistance could completely fulfill the requirements of MD process. PVDF-S-40 ENM presented a prominent permeate vapor flux of 41.1 kg/(m^2·h) due to the optimized MFP resulting from the existence of two special average fiber diameters. Consequently, the desalination evaluation results indicated that the superhydrophobic PVDF-S-*x* ENMs showed superior DCMD performance in the NaCl solution system, which demonstrated the feasibility of designing and manufacturing novel PVDF-S-*x* ENMs for MD applications.

ASSOCIATED CONTENT

Supporting Information

This material is available free of charge via the Internet at http://pubs.acs.org/. The Supporting Information is available free of charge on the ACS Publications website at DOI: 10.1021/acsami.5b06509.

Preparation details of monodisperse silica nanoparticles, FE-SEM images of monodisperse silica nanoparticles with different sizes and size distribution, membrane porosity measurement, liquid entry pressure of water (LEPw) measurement, apparatus for the determination of the LEPw, and schematic diagram of the direct contact membrane distillation (DCMD) setup (PDF)

Video of breathable performance of PVDF-S-40 ENM by observing the color change of methyl orange pH indicator droplet on a hydrochloric acid vial surface that is covered with the membrane (AVI)

AUTHOR INFORMATION

Corresponding Author

*Tel.: +86-21-67792860. Fax: +86-21-67792855. E-mail: wangxf@dhu.edu.cn.

Notes

The authors declare no competing financial interest.

ACKNOWLEDGMENTS

This work was supported by National Science Foundation of China (Grants 51273042 and 21174028), the Program for New Century Excellent Talents in University, the Innovation Program of the Shanghai Municipal Education Commission, the Program of Changjiang Scholars and Innovative Research Team in University (Grant IRT1221), and the Chinese Universities Scientific Fund.

REFERENCES

(1) Shannon, M. A.; Bohn, P. W.; Elimelech, M.; Georgiadis, J. G.; Marinas, B. J.; Mayes, A. M. Science and Technology for Water Purification in the Coming Decades. *Nature* **2008**, *452*, 301−310.

(2) Elimelech, M.; Phillip, W. A. The Future of Seawater Desalination: Energy, Technology, and the Environment. *Science* **2011**, *333*, 712−717.

(3) Fritzmann, C.; Löwenberg, J.; Wintgens, T.; Melin, T. State-of-the-Art of Reverse Osmosis Desalination. *Desalination* **2007**, *216*, 1−76.

(4) Greenlee, L. F.; Lawler, D. F.; Freeman, B. D.; Marrot, B.; Moulin, P. Reverse Osmosis Desalination: Water Sources, Technology, and Today's Challenges. *Water Res.* **2009**, *43*, 2317−2348.

(5) Lawson, K. W.; Lloyd, D. R. Membrane Distillation. *J. Membr. Sci.* **1997**, *124*, 1−25.

(6) Khayet, M. Membranes and Theoretical Modeling of Membrane Distillation: A Review. *Adv. Colloid Interface Sci.* **2011**, *164*, 56−88.

(7) Alkhudhiri, A.; Darwish, N.; Hilal, N. Membrane Distillation: A Comprehensive Review. *Desalination* **2012**, *287*, 2−18.

(8) Koschikowski, J.; Wieghaus, M.; Rommel, M. Solar Thermal-Driven Desalination Plants Based on Membrane Distillation. *Desalination* **2003**, *156*, 295−304.

(9) Kim, Y.-D.; Thu, K.; Ghaffour, N.; Ng, K. C. Performance Investigation of a Solar-Assisted Direct Contact Membrane Distillation System. *J. Membr. Sci.* **2013**, *427*, 345−364.

(10) El-Bourawi, M.; Ding, Z.; Ma, R.; Khayet, M. A Framework for Better Understanding Membrane Distillation Separation Process. *J. Membr. Sci.* **2006**, *285*, 4−29.

(11) Ma, Z.; Hong, Y.; Ma, L.; Su, M. Superhydrophobic Membranes with Ordered Arrays of Nanospiked Microchannels for Water Desalination. *Langmuir* **2009**, *25*, 5446−5450.

(12) Phattaranawik, J.; Jiraratananon, R.; Fane, A. Effect of Pore Size Distribution and Air Flux on Mass Transport in Direct Contact Membrane Distillation. *J. Membr. Sci.* **2003**, *215*, 75−85.

(13) Schofield, R.; Fane, A.; Fell, C.; Macoun, R. Factors Affecting Flux in Membrane Distillation. *Desalination* **1990**, *77*, 279−294.

(14) Ortiz de Zárate, J. M.; Peña, L.; Mengual, J. Characterization of Membrane Distillation Membranes Prepared by Phase Inversion. *Desalination* **1995**, *100*, 139−148.

(15) Matsuura, T. *Synthetic Membranes and Membrane Separation Processes*; CRC Press: Boca Raton, FL, USA, 1994.

DOI: 10.1021/acsami.5b06509
ACS Appl. Mater. Interfaces 2015, 7, 21919−21930

(16) Kujawa, J.; Cerneaux, S.; Koter, S.; Kujawski, W. Highly Efficient Hydrophobic Titania Ceramic Membranes for Water Desalination. *ACS Appl. Mater. Interfaces* **2014**, *6*, 14223−14230.
(17) Lloyd, D. R.; Kinzer, K. E.; Tseng, H. Microporous Membrane Formation Via Thermally Induced Phase Separation. I. Solid-Liquid Phase Separation. *J. Membr. Sci.* **1990**, *52*, 239−261.
(18) Dzenis, Y. Spinning Continuous Fibers for Nanotechnology. *Science* **2004**, *304*, 1917−1919.
(19) Essalhi, M.; Khayet, M. Self-Sustained Webs of Polyvinylidene Fluoride Electrospun Nanofibers at Different Electrospinning Times: 1. Desalination by Direct Contact Membrane Distillation. *J. Membr. Sci.* **2013**, *433*, 167−179.
(20) Wang, X.; Ding, B.; Yu, J.; Wang, M. Engineering Biomimetic Superhydrophobic Surfaces of Electrospun Nanomaterials. *Nano Today* **2011**, *6*, 510−530.
(21) Feng, C.; Khulbe, K. C.; Matsuura, I.; Gopal, R.; Kaur, S.; Ramakrishna, S.; Khayet, A. Production of Drinking Water from Saline Water by Air-Gap Membrane Distillation Using Polyvinylidene Fluoride Nanofiber Membrane. *J. Membr. Sci.* **2008**, *311*, 1−6.
(22) Liao, Y.; Wang, R.; Tian, M.; Qiu, C.; Fane, A. G. Fabrication of Polyvinylidene Fluoride (PVDF) Nanofiber Membranes by Electrospinning for Direct Contact Membrane Distillation. *J. Membr. Sci.* **2013**, *425-426*, 30−39.
(23) Essalhi, M.; Khayet, M. Self-Sustained Webs of Polyvinylidene Fluoride Electrospun Nano-Fibers: Effects of Polymer Concentration and Desalination by Direct Contact Membrane Distillation. *J. Membr. Sci.* **2014**, *454*, 133−143.
(24) Prince, J. A.; Singh, G.; Rana, D.; Matsuura, T.; Anbharasi, V.; Shanmugasundaram, T. S. Preparation and Characterization of Highly Hydrophobic Poly(Vinylidene Fluoride) - Clay Nanocomposite Nanofiber Membranes (PVDF-Clay NNMs) for Desalination Using Direct Contact Membrane Distillation. *J. Membr. Sci.* **2012**, *397−398*, 80−86.
(25) Lalia, B. S.; Guillen-Burrieza, E.; Arafat, H. A.; Hashaikeh, R. Fabrication and Characterization of Polyvinylidenefluoride-Co-Hexafluoropropylene (PVDF-HFP) Electrospun Membranes for Direct Contact Membrane Distillation. *J. Membr. Sci.* **2013**, *428*, 104−115.
(26) Lalia, B. S.; Guillen, E.; Arafat, H. A.; Hashaikeh, R. Nanocrystalline Cellulose Reinforced PVDF-HFP Membranes for Membrane Distillation Application. *Desalination* **2014**, *332*, 134−141.
(27) Liao, Y.; Wang, R.; Fane, A. G. Engineering Superhydrophobic Surface on Poly(Vinylidene Fluoride) Nanofiber Membranes for Direct Contact Membrane Distillation. *J. Membr. Sci.* **2013**, *440*, 77−87.
(28) Dong, Z.-Q.; Ma, X.-h.; Xu, Z.-L.; You, W.-T.; Li, F.-b. Superhydrophobic PVDF-PTFE Electrospun Nanofibrous Membranes for Desalination by Vacuum Membrane Distillation. *Desalination* **2014**, *347*, 175−183.
(29) Liao, Y.; Wang, R.; Fane, A. G. Fabrication of Bioinspired Composite Nanofiber Membranes with Robust Superhydrophobicity for Direct Contact Membrane Distillation. *Environ. Sci. Technol.* **2014**, *48*, 6335−6341.
(30) Liao, Y.; Loh, C.-H.; Wang, R.; Fane, A. G. Electrospun Superhydrophobic Membranes with Unique Structures for Membrane Distillation. *ACS Appl. Mater. Interfaces* **2014**, *6*, 16035−16048.
(31) Tijing, L. D.; Woo, Y. C.; Johir, M. A. H.; Choi, J.-S.; Shon, H. K. A Novel Dual-Layer Bicomponent Electrospun Nanofibrous Membrane for Desalination by Direct Contact Membrane Distillation. *Chem. Eng. J.* **2014**, *256*, 155−159.
(32) Prince, J.; Anbharasi, V.; Shanmugasundaram, T.; Singh, G. Preparation and Characterization of Novel Triple Layer Hydrophilic-Hydrophobic Composite Membrane for Desalination Using Air Gap Membrane Distillation. *Sep. Purif. Technol.* **2013**, *118*, 598−603.
(33) Zhou, T.; Yao, Y.; Xiang, R.; Wu, Y. Formation and Characterization of Polytetrafluoroethylene Nanofiber Membranes for Vacuum Membrane Distillation. *J. Membr. Sci.* **2014**, *453*, 402−408.
(34) Guo, F.; Servi, A.; Liu, A.; Gleason, K. K.; Rutledge, G. C. Desalination by Membrane Distillation Using Electrospun Polyamide Fiber Membranes with Surface Fluorination by Chemical Vapor Deposition. *ACS Appl. Mater. Interfaces* **2015**, *7*, 8225−8232.
(35) Maab, H.; Francis, L.; Al-Saadi, A.; Aubry, C.; Ghaffour, N.; Amy, G.; Nunes, S. P. Synthesis and Fabrication of Nanostructured Hydrophobic Polyazole Membranes for Low-Energy Water Recovery. *J. Membr. Sci.* **2012**, *423−424*, 11−19.
(36) Ma, H.; Burger, C.; Hsiao, B. S.; Chu, B. Ultra-Fine Cellulose Nanofibers: New Nano-Scale Materials for Water Purification. *J. Mater. Chem.* **2011**, *21*, 7507−7510.
(37) Li, X.; Wang, C.; Yang, Y.; Wang, X.; Zhu, M.; Hsiao, B. S. Dual-Biomimetic Superhydrophobic Electrospun Polystyrene Nanofibrous Membranes for Membrane Distillation. *ACS Appl. Mater. Interfaces* **2014**, *6*, 2423−30.
(38) Crespy, D.; Friedemann, K.; Popa, A. M. Colloid-Electrospinning: Fabrication of Multicompartment Nanofibers by the Electrospinning of Organic or/and Inorganic Dispersions and Emulsions. *Macromol. Rapid Commun.* **2012**, *33*, 1978−1995.
(39) Lim, J.-M.; Yi, G.-R.; Moon, J. H.; Heo, C.-J.; Yang, S.-M. Superhydrophobic Films of Electrospun Fibers with Multiple-Scale Surface Morphology. *Langmuir* **2007**, *23*, 7981−7989.
(40) Kanehata, M.; Ding, B.; Shiratori, S. Nanoporous Ultra-High Specific Surface Inorganic Fibres. *Nanotechnology* **2007**, *18*, 315602.
(41) Stöber, W.; Fink, A.; Bohn, E. Controlled Growth of Monodisperse Silica Spheres in the Micron Size Range. *J. Colloid Interface Sci.* **1968**, *26*, 62−69.
(42) Zhang, J.; Zhan, P.; Wang, Z.; Zhang, W.; Ming, N. Preparation of Monodisperse Silica Particles with Controllable Size and Shape. *J. Mater. Res.* **2003**, *18*, 649−653.
(43) Zou, H.; Wu, S.; Shen, J. Polymer/Silica Nanocomposites: Preparation, Characterization, Properties, and Applications. *Chem. Rev.* **2008**, *108*, 3893−3957.
(44) Jena, A.; Gupta, K. Characterization of Pore Structure of Filtration Media. *Fluid/Part. Sep. J.* **2002**, *14*, 227−241.
(45) Dullien, F. A. *Porous Media: Fluid Transport and Pore Structure*, 2nd ed.; Academic Press: London, 1991.
(46) Smolders, K.; Franken, A. C. M. Terminology for Membrane Distillation. *Desalination* **1989**, *72*, 249−262.
(47) Gao, N.; Yan, Y. Characterisation of Surface Wettability Based on Nanoparticles. *Nanoscale* **2012**, *4*, 2202−2218.
(48) Feng, X.; Jiang, L. Design and Creation of Superwetting/Antiwetting Surfaces. *Adv. Mater.* **2006**, *18*, 3063−3078.
(49) Lafuma, A.; Quere, D. Superhydrophobic States. *Nat. Mater.* **2003**, *2*, 457−460.
(50) Wang, L.; Pai, C.-L.; Boyce, M. C.; Rutledge, G. C. Wrinkled Surface Topographies of Electrospun Polymer Fibers. *Appl. Phys. Lett.* **2009**, *94*, 151916−151916−3.
(51) Shin, Y. M.; Hohman, M. M.; Brenner, M. P.; Rutledge, G. C. Electrospinning: A Whipping Fluid Jet Generates Submicron Polymer Fibers. *Appl. Phys. Lett.* **2001**, *78*, 1149−1151.
(52) Wang, J.; Raza, A.; Si, Y.; Cui, L.; Ge, J.; Ding, B.; Yu, J. Synthesis of Superamphiphobic Breathable Membranes Utilizing SiO_2 Nanoparticles Decorated Fluorinated Polyurethane Nanofibers. *Nanoscale* **2012**, *4*, 7549−7556.
(53) Ding, B.; Lin, J.; Wang, X.; Yu, J.; Yang, J.; Cai, Y. Investigation of Silica Nanoparticle Distribution in Nanoporous Polystyrene Fibers. *Soft Matter* **2011**, *7*, 8376−8383.
(54) Liu, M.; Zheng, Y.; Zhai, J.; Jiang, L. Bioinspired Super-antiwetting Interfaces with Special Liquid-Solid Adhesion. *Acc. Chem. Res.* **2010**, *43*, 368−377.
(55) Ra, E. J.; Kim, T. H.; Yu, W. J.; An, K. H.; Lee, Y. H. Ultramicropore Formation in Pan/Camphor-Based Carbon Nanofiber Paper. *Chem. Commun.* **2010**, *46*, 1320−1322.
(56) Lee, K. H.; Kim, H. Y.; Ryu, Y. J.; Kim, K. W.; Choi, S. W. Mechanical Behavior of Electrospun Fiber Mats of Poly (Vinyl Chloride)/Polyurethane Polyblends. *J. Polym. Sci., Part B: Polym. Phys.* **2003**, *41*, 1256−1262.
(57) Tang, X.; Si, Y.; Ge, J.; Ding, B.; Liu, L.; Zheng, G.; Luo, W.; Yu, J. In Situ Polymerized Superhydrophobic and Superoleophilic Nanofibrous Membranes for Gravity Driven Oil-Water Separation. *Nanoscale* **2013**, *5*, 11657−11664.

DOI: 10.1021/acsami.5b06509
ACS Appl. Mater. Interfaces 2015, 7, 21919−21930